

# Optodynamic phenomena in aggregates of polydisperse plasmonic nanoparticles

A. E. Ershov · A. P. Gavriluk ·  
S. V. Karpov · P. N. Semina

Received: 27 May 2013 / Accepted: 30 August 2013 / Published online: 26 September 2013  
© Springer-Verlag Berlin Heidelberg 2013

**Abstract** We propose an optodynamical model of interaction of pulsed laser radiation with aggregates of spherical metallic nanoparticles embedded into host media. The model takes into account polydispersity of particles, pair interactions between the particles, dissipation of absorbed energy, heating and melting of the metallic core of particles and of their polymer adsorption layers, and heat exchange between electron and ion components of the particle material as well as heat exchange with the interparticle medium. Temperature dependence of the electron relaxation constant of the particle material and the effect of this dependence on interaction of nanoparticles with laser radiation are first taken into consideration. We study in detail light-induced processes in the simplest resonant domains of multiparticle aggregates consisting of two particles of an arbitrary size in aqueous medium. Optical interparticle forces are realized due to the light-induced dipole interaction. The dipole moment of each particle is calculated by the coupled dipole method (with correction for the effect of higher multipoles). We determined the role of various interrelated factors leading to photomodification of resonant domains and found an essential difference in the photomodification mechanisms between polydisperse and monodisperse nanostructures.

## 1 Introduction

The studying of nanocomposite materials containing aggregates of plasmonic nanoparticles gains importance due to the unique optical properties and strong dependence of the materials on the local structure of aggregates, which allows these properties to be controlled and offers a great application potential [1–5].

Aggregates with a locally anisotropic structure are capable to immensely enhance spatially localized electromagnetic fields within an inhomogeneously broadened plasmon absorption band near particles resonant to the external electromagnetic field due to the high-Q surface plasmon resonance of nanoparticles.

Over the past decades, a large number of experimental studies have been carried out on the interaction of pulsed laser radiation with composite materials and nanocolloids containing aggregates of metal nanoparticles. Various nonlinear optical effects such as photochromic processes were found and investigated in these media. Most of the obtained results have not yet been adequately explained due to complexity of the accompanying processes. These processes involve interrelated thermodynamic, optical, chemical, mechanical, and other phenomena caused by the impact of optical radiation.

A review of experimental data, in particular, on the giant four-wave degenerated mixing in Ag nanocolloids containing aggregates of nanoparticles compared to non-aggregated nanocolloids can be found in [6]. The review also covers papers on nonlinear optical activity, self-rotation of the polarization ellipse, nonlinear absorption, the inverse Faraday effect, the optical Kerr effect, nonlinear refraction, harmonic generation, enhanced nonlinear optical effect of complex organic molecules adsorbed by the surface of Ag particle, and photochromic reactions underlying the optical memory effect in Ag-dielectric nanocomposites.

---

A. E. Ershov · S. V. Karpov (✉) · P. N. Semina  
L.V. Kirenski Institute of Physics, Russian Academy  
of Sciences, 660036 Krasnoyarsk, Russia  
e-mail: karpov@iph.krasn.ru

A. P. Gavriluk  
Institute of Computational Modeling, Russian Academy  
of Sciences, 660036 Krasnoyarsk, Russia

A. P. Gavriluk · S. V. Karpov  
Siberian Federal University, 660028 Krasnoyarsk, Russia

However, one of the problems yet to be solved is the lack of a complete understanding of dominant mechanisms of nonlinear optical responses. We found that one of the reasons for optical nonlinearity is the effect of spectral-selective transparency of aggregated nanocolloids and nanocomposites under the action of laser pulses. This photochromic effect was first observed in [7] and experimentally investigated in more detail in [8, 9, 10, 11]. The effect is observed when the pulsed laser frequency is within the plasmon absorption band of aggregates, which significantly contributes to the fast optical response.

The optical memory effect is also associated with laser photomodification of nanoaggregates, i.e., modification of local characteristics of aggregates, affecting the plasmon absorption spectrum of aggregates. It is believed that this process is accompanied by a selective change in the structure of resonant domains [12].

The concept of a resonant domain of a multiparticle colloidal aggregate was introduced, in particular, in [13, 14]. The resonant domain is a single particle of an aggregate individually surrounded by other particles and electro-dynamically interacting with them in an external optical field. This affects resonant spectral characteristics of the particle. The resonant frequency of the particle depends on interparticle gaps and the geometry of its immediate surrounding by other particles. The inhomogeneously broadened extinction spectrum of a multiparticle aggregate is a series of resonant bands distributed over a wide spectral range and corresponding to resonant domains of the aggregate.

If the geometry of local environment of particles in a domain changes under the influence of an external optical field, spectral characteristics of the domain change too. Dynamically changing spectral characteristics of a two-particle simplest domain undergoing photomodification in pulsed laser fields are investigated in [6, 15].

Alteration of the domain resonant properties (frequency shift of the maximum in its extinction spectrum dynamically varying during the laser pulse) may be due to both rearrangement of relative positions of neighboring particles and changes in the size, shape, and phase state of the resonant particles (their melting or evaporation). The possibility of light-induced shift of particles in aggregates is discussed in [6, 15–19]. Such a spatial shift is accompanied by the spectral shift of plasmon resonances. One of the reasons for this shift may be the collapsed particle adsorption layer (adlayer hereinafter) as well as photo- or thermoelectron emission from the metallic core [20].

Such processes associated with movement of nanoparticles under the influence of optical radiation fall under the term *optodynamics*. This term used in [20] and in earlier publications by the same authors (e.g., [21, 22]) was introduced to describe a wide range of optically induced mechanical movements and dynamic phenomena that play

an important role in different materials including nanocolloids exposed to laser radiation.

To analyze the regularities observed in nonlinear refraction and nonlinear absorption of colloids, a detailed study on the particle response to external laser irradiation of the aggregate is required taking into account the processes at the interface. These experimental regularities, in particular, include change of the sign of nonlinear refraction with increasing aggregation of silver hydrosol [9, 12, 23] at the wavelength 1.064 micron. However, comprehensive understanding of the physical mechanisms underlying photomodification has not been gained yet.

Another important aspect of the problem that attracts increasing attention [24] is the concept of manipulating light flows at subwavelength scales by using plasmonic materials based on aggregates of metal nanoparticles and fabrication of metamaterials on that basis. In particular, aggregates such as ordered chains of plasmonic nanoparticles are considered to be promising optical waveguides. It is important to have an idea how stable the structure of such aggregates (or irradiated fragments) can remain, since any change in the geometric arrangement of particles will entail changes in their transmission and resonant properties [25–27].

The aim of our paper is to develop a mathematical model to describe the group of interrelated physical processes occurring in resonant domains of multiparticle aggregates and employ this model to study optodynamical processes in these domains (in the form of dimers of metallic nanoparticles) taking into account their polydispersity. Another goal of this paper is to study the mechanisms of fast nonlinear optical responses and photochromic effects in nanoparticle aggregates in metal colloids and nanocomposites containing such aggregates.

The model of interaction of pulsed laser radiation with aggregates of plasmonic nanoparticles describes light-induced changes in the structure of aggregates. The model is based on Brownian dynamics and takes into account interparticle (van der Waals, optical and elastic) interactions, energy dissipation, heat exchange between electron and ion (crystal lattice) components of the particle material as well as between the particles and the surrounding medium, and the heating and melting of polymer adsorption layers of particles. Dipole optical interactions of particles in restructuring aggregate at each iteration step are realized using the coupled dipole method. The role of various factors (including the effect of optical forces) leading to photomodification of resonant domains in picosecond laser pulses is established.

The paper is organized as follows. In Sect. 2, we describe the optodynamical model and the interactions taken into account as well as the factors accompanying the effect of picosecond pulsed laser radiation on resonant domain. In Sect. 3, we perform simulation with our model

for a silver nanoparticle dimer as a classical material of nanoplasmonics.

## 2 Model

In this paper, we propose a modified model of interaction of pulsed laser radiation with aggregates consisting of an arbitrary number of particles. The model is supplemented with a few new important factors. Unlike the previous version [6], our new model makes it possible to analyze light-induced interactions in multiparticle aggregates with an arbitrary geometry, number of particles, and their relative sizes. Polydispersity of particles in aggregates inherent in experimental objects was taken into consideration as well as temperature dependence of the resonant properties of particles (in particular, the dependence of the free electron relaxation constant of the particle material on temperature and the physical state on) including the effect of melting on domain properties. These factors are shown to be important and play a key role in the photomodification process. It makes the model adequate for simulation of real processes occurring in nanocolloids.

We apply our model to analyze all interactions and processes taking place in real colloidal aggregates using the simplest type of resonant domains [6, 14] in the form of dimers. In general, each particle in an aggregate is under the action of a resultant force including van der Waals  $(\mathbf{F}_{vdw})_i$ , elastic  $(\mathbf{F}_{el})_i$ , optical  $(\mathbf{F}_{opt})_i$ , viscous  $(\mathbf{F}_v)_i$  forces, and the interparticle  $(\mathbf{F}_f)_i$  friction force. In the next subsections, we consider these interactions in detail.

### 2.1 Elastic interaction

The elastic force  $(\mathbf{F}_{el})_i$  exerted on the  $i$ th particle by other particles because of deformation of the adsorption layers of contacting particles can be expressed in terms of the pair potential energy of elastic interaction  $U_{el}$ :

$$(\mathbf{F}_{el})_i = -\frac{\partial U_{el}}{\partial \mathbf{r}_i}, \quad U_{el} = \frac{1}{2} \sum_{i=1}^N \sum_{\substack{j=1 \\ j \neq i}}^N (U_{el})_{ij}. \quad (1)$$

The potential energy  $(U_{el})_{ij}$  of elastic interaction between two adsorption layers (neglecting the Poisson ratio) is given by an expression [28] obtained on the basis of the Hertz problem of deformation of two touching spheres [29]:

$$(U_{el})_{ij} = \frac{8}{15} (h_i + h_j - h_{ij})^{5/2} \left[ \frac{(R_i + h_i)(R_j + h_j)}{R_i + h_i + R_j + h_j} \right]^{1/2} \frac{(E_{el})_i \cdot (E_{el})_j}{(E_{el})_i + (E_{el})_j} H(h_i + h_j - h_{ij}), \quad (2)$$

where  $h_{ij} = |\mathbf{r}_{ij}| - (R_i + R_j)$  is the interparticle gap:  $\mathbf{r}_{ij} = \mathbf{r}_i - \mathbf{r}_j$  is the vector joining the centers of the particles,  $R_i, R_j$  are the particle radii,  $H(x)$  is the Heaviside function,  $h_i, h_j$  are the thicknesses of undeformed particle adsorption layers, and  $(E_{el})_i, (E_{el})_j$  are the effective elasticity moduli of particle adlayers; their value is determined from the force balance. The Heaviside function introduced in (2) accounts for the fact that the elastic interaction energy is zero when adlayers are not in contact.

Equation (2) can also describe the elastic interaction of particles when one (or both) of them have no elastic adlayers ( $h_i = 0$ ). In this case, we can use the elasticity modulus of the metallic core instead of that of polymer adlayers.

### 2.2 The van der Waals interaction

The van der Waals force acting on each  $i$ th particle  $(\mathbf{F}_{vdw})_i$  consists of the van der Waals forces of all  $j$ -th particles acting on the  $i$ -th one and is expressed in terms of potential energy  $U_{vdw}$ :

$$(\mathbf{F}_{vdw})_i = -\frac{\partial U_{vdw}}{\partial \mathbf{r}_i}, \quad U_{vdw} = \frac{1}{2} \sum_{i=1}^N \sum_{\substack{j=1 \\ j \neq i}}^N (U_{vdw})_{ij} \quad (3)$$

The total potential energy of the van der Waals interaction  $U_{vdw}$  is a sum of the pair interaction energies  $(U_{vdw})_{ij}$  described by the expression [30]:

$$(U_{vdw})_{ij} = -\frac{A_H}{6} \left( \frac{2R_i R_j}{h_{ij}^2 + 2R_i h_{ij} + 2R_j h_{ij}} + \frac{2R_i R_j}{h_{ij}^2 + 2R_i h_{ij} + 2R_j h_{ij} + 4R_i R_j} + \ln \frac{h_{ij}^2 + 2R_i h_{ij} + 2R_j h_{ij}}{h_{ij}^2 + 2R_i h_{ij} + 2R_j h_{ij} + 4R_i R_j} \right) \quad (4)$$

Here,  $A_H \approx 50k_B T$  is the Hamaker constant for silver hydrosol,  $k_B$  is the Boltzmann constant,  $T$  is the temperature,  $R_i$  and  $R_j$  are the particle radii.

In our model, we ignore the electrostatic interaction of particles associated with overlapping of electric double layers (EDL) consisting of electrolyte ions adsorbed on a particle because the nanocolloids used in the experiments had thin EDL in the interparticle medium with a high electrolyte concentration. It was shown in [4, 20] that under such conditions, EDL are located near the particle surface in the bottom part of the polymer adlayer where the van der Waals forces dominate.

### 2.3 Dissipative forces of viscous and tangential friction

Viscous friction forces acting on a particle moving in a viscous medium with the velocity  $\mathbf{v}_i$  obey the Stokes law:

$$(\mathbf{F}_v)_i = -6\pi\eta(R_i + h_i)\mathbf{v}_i, \quad (5)$$

where  $\eta$  is the temperature dependent dynamical viscosity of the interparticle medium.

Tangential friction forces occur when particles in aggregate move transversally relative to each other. Simplistically, they can be described by analogy with the forces of dry friction (although they are not the ones). The coefficient of friction is an effective parameter that characterizes the degree of interaction between the touching particles adlayers. Because of strong intermolecular interaction of particles adlayers and their non-uniform deformation, the effective coefficient of friction can significantly exceed unity.

The direction of tangential friction force is opposite to the projection of the relative velocity of particles ( $\mathbf{v}_j - \mathbf{v}_i$ ) on the plane of adlayers contact. Thus, the tangential friction force exerted on the  $i$ th particle by the  $j$ th particle is determined by the following expression:

$$(\mathbf{F}_f)_{ij} = -\mu |(\mathbf{F}_{el})_{ij}| \mathbf{q}_{ij}, \quad (6)$$

where  $\mu$  is the effective friction coefficient,  $\mathbf{q}_{ij}$  is the normalized vector of the projection of particles' relative velocity on the plane of contact of particle adlayers:

$$\mathbf{q}_{ij} = \frac{(\mathbf{v}_j - \mathbf{v}_i) - \mathbf{n}_{ij}((\mathbf{v}_j - \mathbf{v}_i) \cdot \mathbf{n}_{ij})}{|(\mathbf{v}_j - \mathbf{v}_i) - \mathbf{n}_{ij}((\mathbf{v}_j - \mathbf{v}_i) \cdot \mathbf{n}_{ij})|},$$

where  $\mathbf{n}_{ij} = \frac{\mathbf{r}_{ij}}{|\mathbf{r}_{ij}|}$  is the normalized unit vector connecting particle centers.

The total tangential friction force is a sum of friction forces acting on the  $i$ th particle:

$$(\mathbf{F}_f)_i = \sum_{\substack{j=1 \\ i \neq j}}^N (\mathbf{F}_f)_{ij}. \quad (7)$$

#### 2.4 Light-induced optical forces

Optical forces [31] acting on the particle  $i$  from external electromagnetic field and neighboring particles are expressed via the energy of particle interaction with the local field:

$$(\mathbf{F}_{opt})_i = -\frac{\partial U_{opt}}{\partial \mathbf{r}_i}. \quad (8)$$

Potential energy of optical interaction  $U_{opt}$  comprises the energies of interaction of dipole moments  $\mathbf{d}_i$  of each particle with an external field and other particles [31] (see also [16–19]):

$$U_{opt} = -\frac{1}{4} \text{Re} \sum_{i=1}^N \left[ \mathbf{d}_i \cdot \mathbf{E}^*(\mathbf{r}_i) + \frac{1}{2} \mathbf{d}_i \cdot \left( \frac{\mathbf{d}_i}{\varepsilon_0 \alpha_i} - \mathbf{E}(\mathbf{r}_i) \right)^* - \varepsilon_0 \alpha_i |\mathbf{E}_0|^2 \right] \cdot H(\tau - t). \quad (9)$$

Here,  $\mathbf{E}(\mathbf{r}_i)$  is the external field strength at point  $\mathbf{r}_i$  [see (11)],  $\mathbf{E}_0$  is field amplitude, the symbol (\*) denotes complex conjugation,  $\varepsilon_0$  is the permittivity of free space,  $\alpha_i$  is the dipole polarizability of a particle, and  $\tau$  is the laser pulse duration. The first term in (9) describes the energy of interaction of particles in aggregate with an external electromagnetic field. The second term is responsible for the energy of the dipole interaction of particles. The expression in round brackets corresponds to the portion of the local field produced by all particles surrounding the  $i$ th particle of the aggregate; factor  $1/2$  is introduced to avoid double counting of the interaction;  $(\mathbf{d}_i/\varepsilon_0 \alpha_i)$  is the local field. The third term is the energy of interaction of isolated particles with an external field. The Heaviside function allows us to take into account the end of the laser pulse.

Light-induced dipole moments  $\mathbf{d}_i$  of particles are calculated by the coupled dipole method [expression (18)] at each iteration step for current configuration of particles in an aggregate (see, for example, [32]). To simulate the contribution of higher multipoles to light-induced interaction, we introduced a renormalization coefficient  $\xi$  in equations (18), which ensures less than real interparticle distances  $\mathbf{r}_{ij}$  for pairs of adjacent particles [32]. Thus, the center-to-center distances  $\mathbf{r}'_{ij}$  used in the coupled dipole method are defined by the following condition:

$$\mathbf{r}'_{ij} = \begin{cases} \xi^{-1} \mathbf{r}_{ij}, & |\mathbf{r}_{ij}| \leq 1.5(R_i + R_j) \\ \mathbf{r}_{ij}, & |\mathbf{r}_{ij}| > 1.5(R_i + R_j) \end{cases}. \quad (10)$$

The coefficient  $\xi$  is determined from similarity of the computed extinction spectra of Ag nanoparticle aggregates with the corresponding experimental spectra of aggregated Ag colloids. Note that the coupled multipole method ([33]) cannot be used in this model because it requires all particles in an aggregate to have equal permittivity.

An important advantage of our approach is the employment of the modified coupled dipole method to take into account polydispersity of nanoparticles [34] in aggregates since real colloidal aggregates are strongly polydisperse.

In this method, we consider the interaction of a plane electromagnetic wave

$$\mathbf{E}(\mathbf{r}) = \mathbf{E}_0 \exp(i\mathbf{k} \cdot \mathbf{r}) \quad (11)$$

with aggregated spherical nanoparticles interacting with each other and with an external field via fields produced by light-induced dipole moments of other particles. Particle sizes are assumed to be much smaller than the radiation wavelength.

The expression for dipole polarizability of a spherical particle with radius  $R_i$  taking into account the self-action of oscillating dipole and the size effect is [32]:

$$\alpha_i = R_i^3 \frac{\varepsilon_i - \varepsilon_m}{\varepsilon_i + 2\varepsilon_m - \frac{2}{3}i(R_i|\mathbf{k}|)^3(\varepsilon_i - \varepsilon_m)}, \tag{12}$$

where  $\varepsilon_i$  is the dielectric constant of the particle,  $\varepsilon_m$  is the dielectric constant of the interparticle medium, and  $\mathbf{k}$  is the wave vector. The dielectric constant  $\varepsilon_i$  of metal particles dependent on the size, temperature, and physical state is modified according to [1, 32]:

$$\varepsilon_i = \varepsilon_{\text{tab}} + \frac{\omega_p^2}{\omega[\omega - i\Gamma_0]} - \frac{\omega_p^2}{\omega[\omega - i\Gamma_i]}, \tag{13}$$

where  $\omega$  is the frequency of the external electromagnetic wave,  $\omega_p$  is the metal plasma frequency,  $\Gamma_0$  is the relaxation constant of conduction electrons for bulk metal at initial temperature  $T_0$ ,  $\varepsilon_{\text{tab}}$  is the tabulated data on spectral dependence of the dielectric constant of bulk metal at initial temperature  $T_0$  (see, for example. [35]),  $\Gamma_i$  is the relaxation constant for the spherical nanoparticle, depending on its size, temperature, and the physical state of the material. The size dependence of the relaxation constant of the particle material is:

$$\Gamma_i = \Gamma_{\infty,i} + A \frac{v_F}{R_i}, \tag{14}$$

where  $\Gamma_{\infty,i}$  is the relaxation constant of the particle material taking into consideration its temperature and physical state and  $v_F$  is the Fermi velocity. The multiplier  $A$  is assumed to be 1 in the most of optical model calculations. However, generally, relaxation processes at a particle interface depend on the state of its surface and other factors.

In our paper, we take into account an important factor of temperature dependence of the electron relaxation constant and its alteration as the temperature of the particle metal core comes close to the melting temperature. This change is believed to be due to saturation of the crystal lattice with point defects such as vacancies that can become additional scattering centers for conduction electrons causing changes in the optical constants of the particle material [1]. Ultimately, this may lead to a decrease in the Q-factor of the surface plasmon resonance of a particle and to its disappearance when the particle melts (see Fig. 2.12 in [1]). Assuming a linear dependence of the electron–phonon interaction cross section on the particle temperature [36], the relaxation constant is proportional to the metal temperature

$$\Gamma_{\infty,i} \sim (T_i)_i$$

where  $(T_i)_i$  is the temperature of the lattice (ion) component of the  $i$ th particle

Melting of the particle leads to an abrupt growth of the relaxation constant up to the value  $\Gamma_{\text{liq}}$  that corresponds to that of a liquid metal at melting temperature and is taken to

be  $20\Gamma_0$  (see “Appendix”). This magnitude (in the absence of direct data) can be estimated from the temperature dependence of optical constants including the temperature of phase transition and change of reflection coefficients of solid and liquid metals [37, 38]. In our model, the increase in the relaxation constant in the process of melting is approximated by a linear function depending on the fraction of the particle liquid phase, or, in terms of thermal energy, the magnitude  $\Gamma_{\infty,i}$  is defined by the factor:

$$\Gamma_{\infty,i} \sim \frac{(Q_i)_i - (Q_1)_i}{(Q_2)_i - (Q_1)_i}, \quad \begin{aligned} (Q_1)_i &= C_i V_i \cdot T_L(R_i) \\ (Q_2)_i &= (Q_1)_i + L V_i. \end{aligned} \tag{15}$$

where  $(Q_i)_i$  is the thermal energy transferred to the ion component of a particle,  $(Q_1)_i$ ,  $(Q_2)_i$  are the thermal energies at the initial and final stages of melting,  $C_i = 2.5 \times 10^6 \text{ J/m}^3 \text{ K}$  [39] is the volumetric heat capacity of the ion component of the particle material,  $T_L(R_i)$  is the size dependence of the nanoparticle melting temperature,  $L$  is the volumetric heat of melting for metal,  $V_i$  is the nanoparticle volume.

Thus, in these approximations, the relaxation constant of the particle material can be described by the following expression taking into account the size dependence of melting temperature on the particle radius:

$$\Gamma_{\infty,i} = \Gamma_0 \cdot \left[ \frac{(T_i)_i}{T_0} + \frac{(Q_i)_i - (Q_1)_i}{(Q_2)_i - (Q_1)_i} \left( \frac{\Gamma_{\text{liq}}}{\Gamma_0} - \frac{T_L(R_i)}{T_0} \right) H((Q_2)_i - (Q_i)_i) H((Q_i)_i - (Q_1)_i) \right]. \tag{16}$$

where  $T_L(R_i)$  is the size dependence of melting temperature.

The size dependence of melting temperature for a particle with radii  $R_i \geq 2 \text{ nm}$  is approximated by the expression [40] (here  $R_i$  is the radius in nm):

$$T_L(R_i) = T_{L,\infty} \cdot \left( 1 - \frac{1 \text{ nm}}{R_i} \right) \tag{17}$$

where  $T_{L,\infty}$  is the melting temperature of bulk metal (silver, in our case).

The dipole moment of the  $i$ th particle in aggregate interacts with an external field and the fields produced by other ( $j$ )th particles (taking into account polydispersity of the particles) and obeys the coupled dipole equations (see, for example. [32]):

$$d_{i\alpha} = \varepsilon_0 \alpha_i \left( (E_0)_\alpha \exp(i\mathbf{k} \cdot \mathbf{r}_i) + \sum_{\substack{j=1 \\ i \neq j}}^N \sum_{\beta=1}^3 G_{\alpha\beta}(\mathbf{r}'_{ij}) d_{j\beta} \right), \tag{18}$$

for  $\mathbf{r}'_{ij}$  see Eq. (10).

The interparticle interaction tensor  $G_{\alpha\beta}$  in the case when the size of nanoparticle aggregate exceeds the radiation wavelength is given by

$$G_{\alpha\beta}(\mathbf{r}) = |\mathbf{k}|^3 \left( A(|\mathbf{k}||\mathbf{r}|) \delta_{\alpha\beta} + B(|\mathbf{k}||\mathbf{r}|) \frac{r_\alpha r_\beta}{r^2} \right), \quad (19)$$

$$A(X) = (X^{-1} + iX^{-2} - X^{-3}) \exp(iX), \quad (20)$$

$$B(X) = (-X^{-1} - 3iX^{-2} + 3X^{-3}) \exp(iX). \quad (21)$$

where  $\alpha$  and  $\beta$  denote Cartesian components of the vector.

3N-dimensional system of equations (18) is a set of algebraic equations with respect to the Cartesian components of the dipole moment vectors. The solution of this system is a set of complex vectors  $\mathbf{d}_i$  used to calculate the optical properties of nanoparticle aggregate and optical forces [see Eq. (9)].

Extinction cross section is given by the expression

$$\sigma_e = 4\pi |\mathbf{k}| \operatorname{Im} \sum_{i=1}^N \frac{(\mathbf{d}_i \cdot \mathbf{E}^*(\mathbf{r}_i))}{|\mathbf{E}_0|^2}. \quad (22)$$

For extinction efficiency, we have the formula [32]:

$$Q_e = \frac{\sigma_e}{\sum_{i=1}^N \pi R_i^2}. \quad (23)$$

## 2.5 Thermodynamic characteristics of the system and external heat transfer

Heating of nanoparticles under applied laser radiation is a significant factor leading to the change in the optical properties of particles and the characteristics of adlayers. The absorbed power of laser radiation  $W_i$  in the dipole approximation is described by the expression [31]:

$$W_i = \frac{\omega |\mathbf{d}_i|^2}{2\epsilon_0} \operatorname{Im} \left( \frac{1}{\alpha_i^*} \right). \quad (24)$$

Absorption of radiation by the particle results primarily in the heating of free electrons which in turn heats the ionic (lattice) subsystem. The change in the electron component temperature  $(T_e)_i$  due to absorption of electromagnetic energy by the particle and heat exchange with the ion component is described by the expression [6, 39]:

$$(C_e)_i \frac{d(T_e)_i}{dt} = -g[(T_e)_i - (T_i)_i] + \frac{W_i}{V_i}. \quad (25)$$

Here,  $(C_e)_i$  is the volumetric heat capacity of electron components [40]:  $(C_e)_i = 68(T_e)_i \text{ J/m}^3 \text{ K}$ ,  $V_i$  is the particle volume,  $g = 4 \times 10^{16} \text{ J/m}^3 \text{ K s}$  is the rate of energy exchange between the electron and ion subsystems independent of temperature for temperatures higher than the Debye temperature [41–43].

The change of the ion component temperature  $(T_i)_i$  is determined by heat exchange with the electron component and the interparticle medium. To take into account phase

transition (solid–liquid) in particles, a thermal energy equation for the lattice  $(Q_i)$  is used instead of the equation for  $T_i$ :

$$\frac{d(Q_i)_i}{dt} = gV_i[(T_e)_i - (T_i)_i] + (q_1)_i V_i, \quad (26)$$

where  $(q_1)_i$  is the heat flow per unit volume describing thermal losses [6]:

$$(q_1)_i = -\frac{3}{2R_i} (\chi_m c_{m0} \rho_m)^{1/2} \cdot [(T_i)_i - T_0] \cdot t^{-1/2}, \quad (27)$$

$\chi_m$  is the thermal conductivity,  $c_{m0}$  is the heat capacity, and  $\rho_m$  is the interparticle medium density.

The ion component temperature with the account of melting is expressed via  $(Q_i)_i$ :

$$(T_i)_i = \frac{(Q_i)_i}{C_i V_i} H((Q_i)_i - (Q_i)_i) + \frac{(Q_i)_i - (Q_2)_i}{C_i V_i} H((Q_i)_i - (Q_2)_i) + T_L(R_i) H((Q_i)_i - (Q_q)_i). \quad (28)$$

The particle and the interparticle medium are heated when laser radiation is absorbed and this leads to a change in the adlayer elasticity modulus due to destruction of molecular bonds in the polymer grid of the adlayer. This occurs over finite relaxation time  $\tau_r$  and is described by the expression [6, 44]:

$$\tau_r(T) = \tau_0 \exp\left(\frac{U_f}{k_B T}\right). \quad (29)$$

The value of  $\tau_0$  is assumed to be  $10^{-12} \text{ s}$  [6, 44] and  $U_f$  is the energy of chemical bonds in the polymer adlayer (taken to be about 1 eV in our calculations, which is typical of the chemical bond energy of polymers). Taking into account the finite relaxation time, the temperature dependence of the elasticity modulus is described by the following equation [6]:

$$\frac{d(E_{el})_i}{dt} = -\frac{(E_{el})_i}{\tau_r((T_m)_i)}, \quad (30)$$

where  $(T_m)_i$  is the average temperature of the heated area near the  $i$ th particle:

$$(T_m)_i = \frac{(T_i)_i + T_0}{2}, \quad (31)$$

$T_0$  is the temperature of the interparticle medium.

## 2.6 Kinetic equations for domain particles under photomodification

So the following set of differential equations

$$\frac{d\mathbf{r}_i}{dt} = \mathbf{v}_i, \quad (32)$$

$$m_i \frac{d\mathbf{v}_i}{dt} = \mathbf{F}_i, \tag{33}$$

$$\mathbf{F}_i = (\mathbf{F}_{vdw})_i + (\mathbf{F}_{el})_i + (\mathbf{F}_{opt})_i + (\mathbf{F}_v)_i + (\mathbf{F}_f)_i,$$

$$\frac{d(E_{el})_i}{dt} = -\frac{(E_{el})_i}{\tau_r((T_m)_i)}, \tag{34}$$

$$(C_e)_i \frac{d(T_e)_i}{dt} = -g[(T_e)_i - (T_i)_i] + \frac{W_i}{V_i}, \tag{35}$$

$$\frac{d(Q_i)_i}{dt} = gV_i[(T_e)_i - (T_i)_i] + (q_1)_i V_i, \tag{36}$$

$$(T_i)_i = \frac{(Q_i)_i}{C_i V_i} H((Q_1)_i - (Q_i)_i) + \frac{(Q_i)_i - (Q_2)_i}{C_i V_i} H((Q_1)_i - (Q_i)_i) - (Q_i)_i + T_L(R_i) \cdot H((Q_1)_i - (Q_i)_i).$$

and linear algebraic equations (18) provide the basis of the optodynamical model. Equations (32) and (33) describe the dynamics of particles near their positions in the aggregate, and Eq. (34) describes the elasticity modulus of adlayers changing due to heating and destruction of chemical bonds in the polymer. Equations (35) and (36) describe heating and cooling of electron and ion components of the particle material and the heat transfer between them. Since the model takes into account melting of the particle material, description of thermodynamics of the ion component is more appropriate in terms of heat energy than in terms of temperature.

We used the Nordsieck-Gear predictor–corrector method of fifth order to solve system (32) and (33), the Euler method to solve (34), (35), (36), and the method of conjugated gradients to solve system (18).

### 3 Results and discussions

In this section, our model is applied to study optodynamical processes in the simplest type of resonant domains in aggregate: a dimer consisting of two spherical plasmonic Ag nanoparticles embedded in water ( $\epsilon_m = 1.78$ —the case

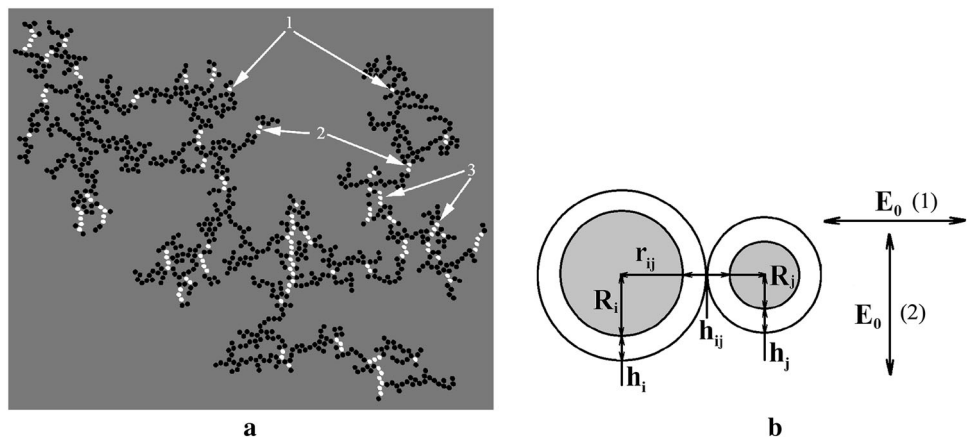
of hydrosols) interacting with pulsed laser radiation of various intensity, polarization, and wavelength. In a general case, orientation of dimers to the laser field polarization can be arbitrary. But in this section, we chose to study resonant domains being parallel to the polarization, since in this case, the photomodification effects are most pronounced (compared to the transversal polarization). The domain characteristics were shown to change insignificantly for transverse polarization under the same conditions (Fig. 1).

Time-dependent characteristics of resonant domains consisting of equal size particles (a monodisperse domain) with the radii  $R_1 = R_2 = 5$  nm and of different-sized particles:  $R_1 = 2$  nm and  $R_2 = 8$  nm (a polydisperse domain) are shown in Figs. 2, 3, 4, 5, and 6. The domain characteristics include extinction spectrum  $Q_e$ , temperatures of the ion and electron components of the particle material, thicknesses  $h_i, h_j$ , and the elasticity modulus  $E_{el}$  of the polymer adlayer. The domain characteristics change under heating and melting of the particle material induced by a laser pulse with  $\tau = 20$  ps, different radiation wavelength, and intensity. In addition, the domain characteristics include the total energy of particle interaction comprising van der Waals  $U_{vdw}$ , elastic  $U_{el}$ , and optical  $U_{opt}$  components (the latter is taken into account while the pulse is on) as well as the total energy  $U_{tot}$  less optical interaction. The initial values of the interparticle gap, thickness, and elasticity modulus of polymer adlayers are, respectively, as follows:  $h_{ij} = 1$  nm,  $h_i = h_j = 0.65$  nm, and  $E_{el} = 3 \times 10^8$  N/m<sup>2</sup> ( $h_{ij} < h_i + h_j$  due to deformation of adlayers in contact). Potential curves at the end of the pulse are given in Figs. 2, 3, 4, 5, and 6.

#### 3.1 Monodisperse domain

First of all, we need to understand how taking into account temperature dependence of the electron relaxation constant of the particle material  $\Gamma_i(T)$  affects kinetics of the domain characteristics in monodisperse dimers.

**Fig. 1** **a** Schematic image of a particle aggregate. Resonant domains with different number of particles (1, 2, 3 and more) are marked with white; **b** polydisperse dimer (as a simplest domain) in longitudinal (1), and transversal (2) polarization



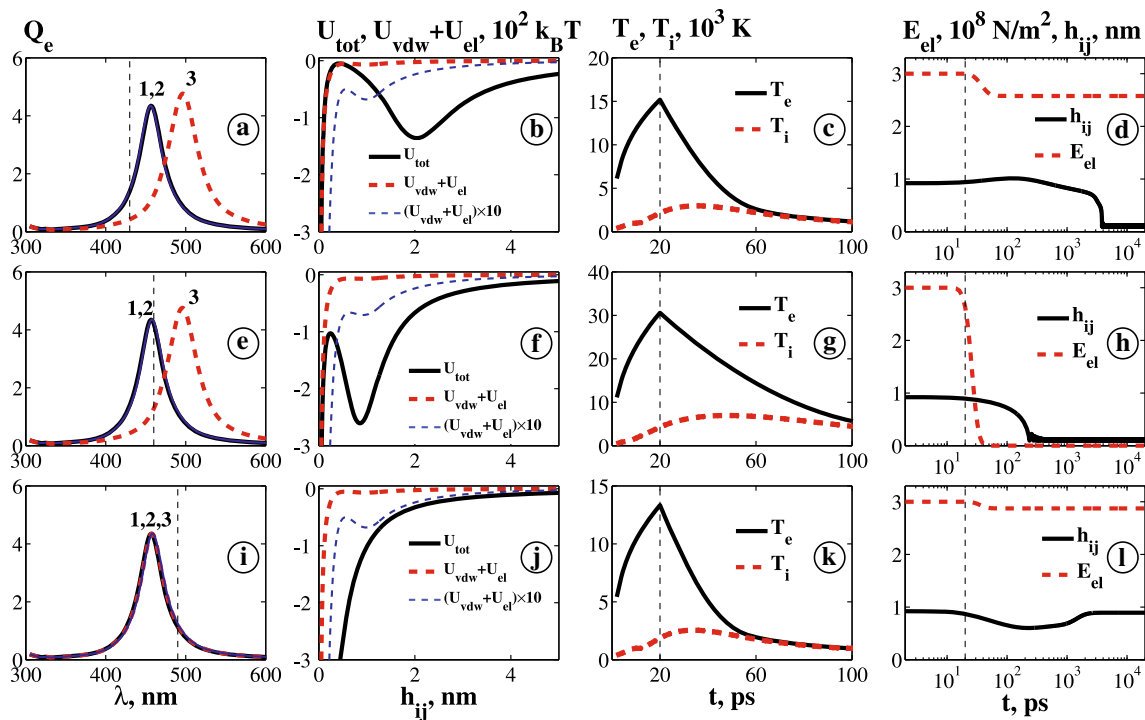


**Fig. 2** Kinetics of the parameters of a monodisperse dimer (the case of  $\Gamma_i = \text{const}$ ). Curves in the extinction spectra  $Q_e(\lambda)$  refer to: 1 ( $t = 0$ ), 2 ( $t = \tau$ ), 3  $t = 20$  ns.  $I = 7.5 \times 10^8$  W/cm<sup>2</sup>

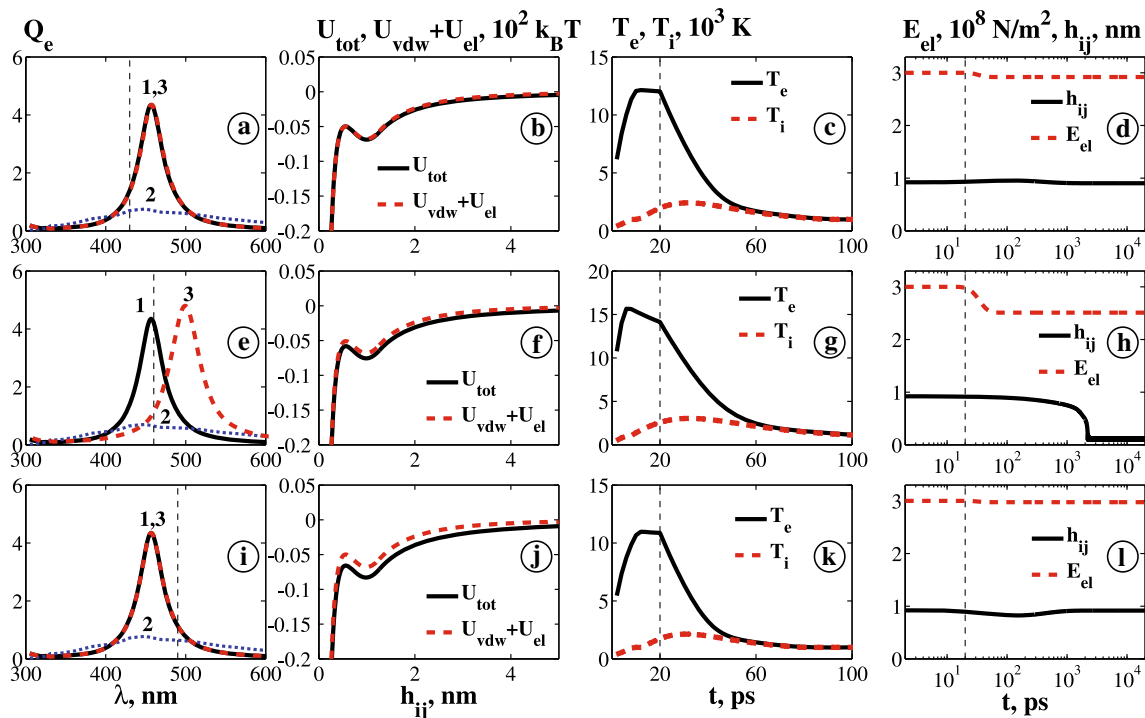


**Fig. 3** Kinetics of the parameters of a monodisperse dimer.  $\Gamma_i = \Gamma_i(T)$ . The rest of the parameters are as in Fig. 2

In Figs. 2 and 3, we show comparative changes in the characteristics of identical monodisperse resonant domains under the action of pulsed laser radiation with the duration

$\tau = 20$  ps, intensity  $I$  of  $7.5 \times 10^8$  W/cm<sup>2</sup> (close to the experimental values), that corresponds to field strength  $5.3 \times 10^7$  V/cm, and the wavelengths (from top to

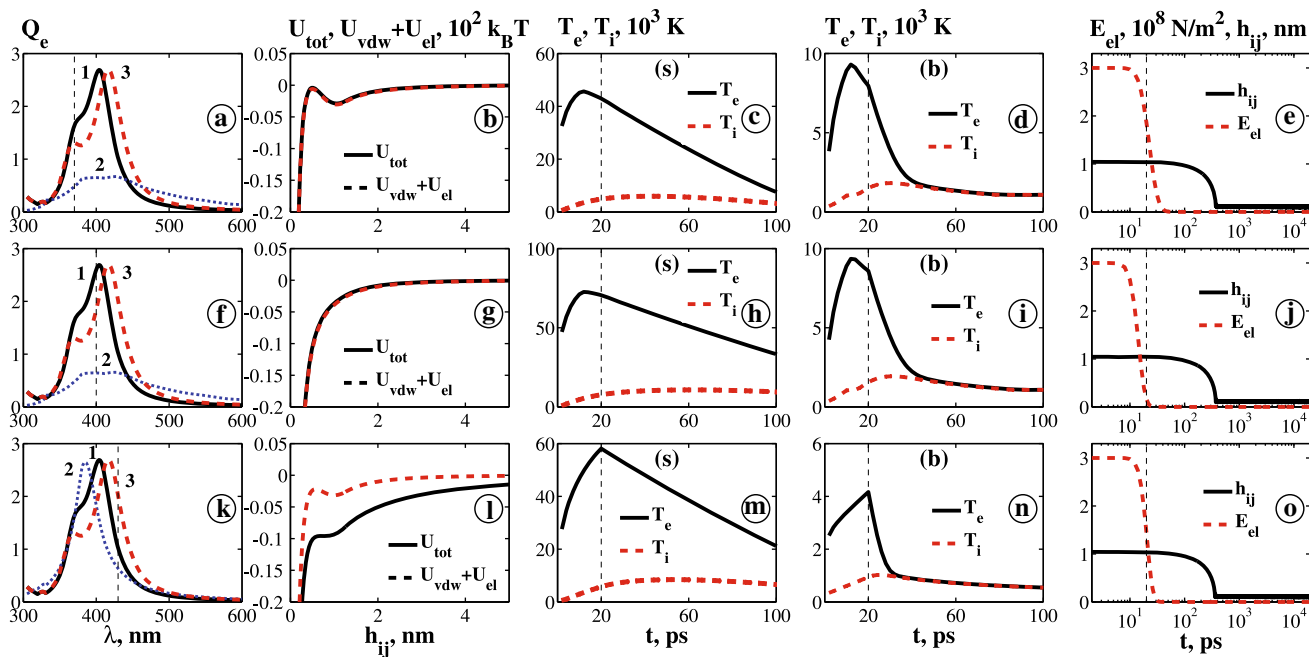


**Fig. 4** Kinetics of polydisperse dimer parameters [the case of  $\Gamma_i(T)$ ]. Extinction spectrum  $Q_e(\lambda)$  for 1 ( $t = 0$ ), 2 ( $t = 20$  ps), 3  $t = 20$  ns. Kinetics of the elasticity modulus of AL  $E_{el,i}$  is presented for a small particle.  $I = 7.5 \times 10^8$  W/cm<sup>2</sup>

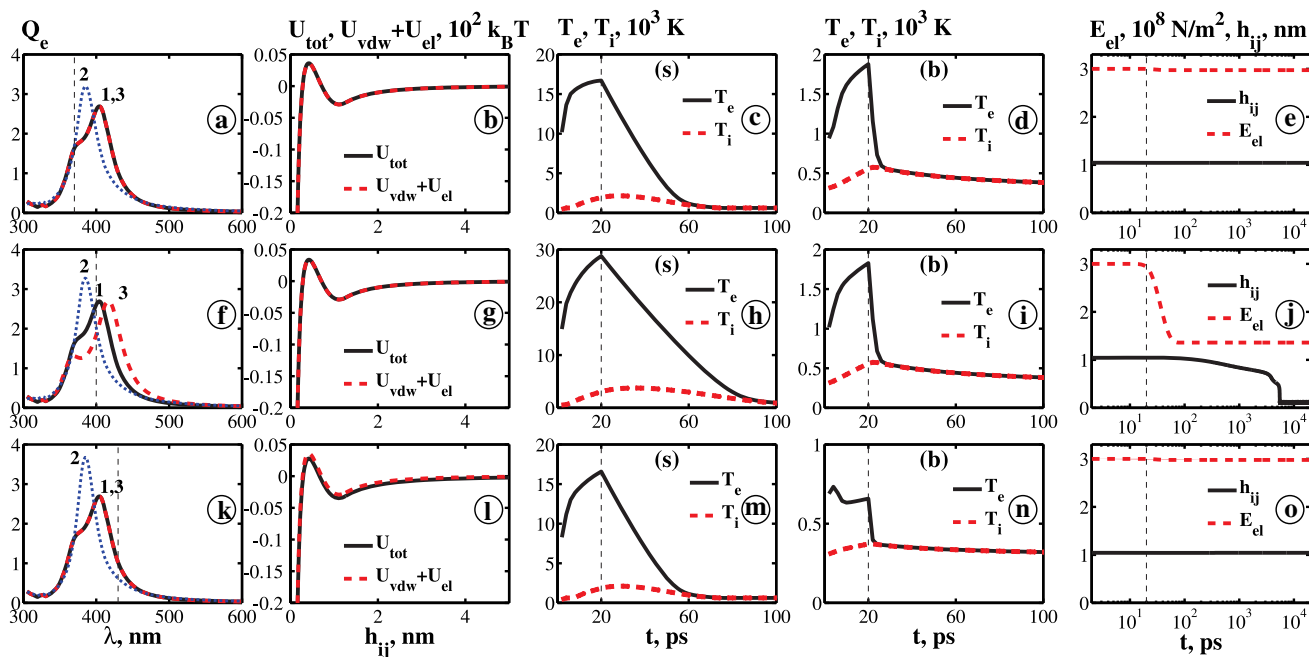


**Fig. 5** Kinetics of polydisperse dimer parameters [the case of  $\Gamma_i(T)$ ]. Extinction spectrum  $Q_e(\lambda)$  for 1 ( $t = 0$ ), 2 ( $t = 20$  ps), 3  $t = 20$  ns. Kinetics of the elasticity modulus of AL  $E_{el,i}$  is presented for a small particle.  $I = 7.7 \times 10^7$  W/cm<sup>2</sup>

bottom):  $\lambda = 430, 460$  and  $490$  nm. The wavelengths to irradiate a monodisperse dimer were chosen to coincide with the short- and long-wavelength wings of the initial extinction spectrum and with its maximum.

The first column in these figures includes extinction spectra  $Q_e$ : initial (curve 1), just after the pulse is over

( $t = \tau$ , curve 2) and long time after the pulse is over ( $t = 20$  ns, curve 3). The second column contains the total energy  $U_{tot}$  and  $U_{tot}$  less optical interaction  $U_{opt}$ . The third column illustrates temperature dynamics of the ion  $T_i$  and electron  $T_e$  subsystems of the metal core. The fourth column shows temporal change of the elasticity modulus  $E_{el}$

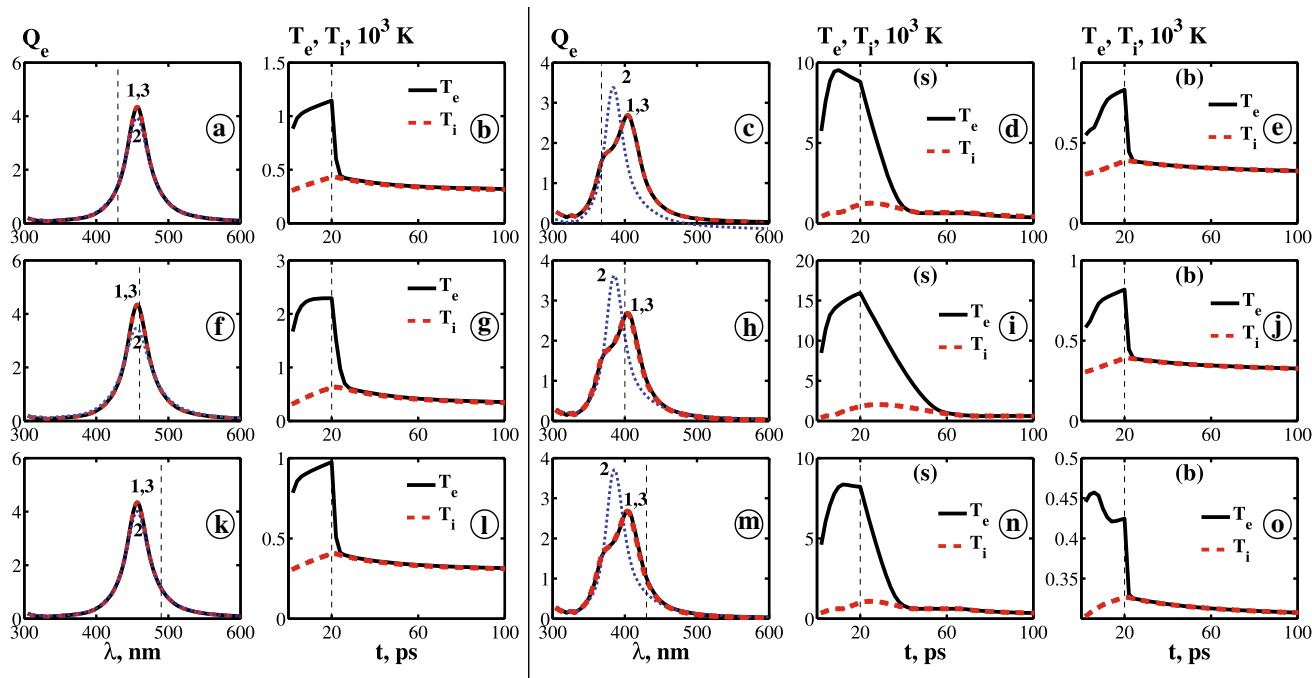


**Fig. 6** Kinetics of parameters for monodisperse (a, b, f, g, k, l) and polydisperse dimers (c, d, e, h, i, j, m, n, o) (the case of  $\Gamma_i(T)$ ).  $I = 2.7 \times 10^7 \text{ W/cm}^2$

of polymer adlayers and the interparticle gap  $h_{ij}$  (vertical dash lines in the forth column correspond to the pulse end).

To estimate the effect of varying  $\Gamma_i$  on the properties of dimers, calculations were made ignoring the change of the relaxation constant ( $\Gamma_i = \text{const}$ ) (Fig. 2) and for the case when  $\Gamma_i(T)$  (Fig. 3). As can be seen from Fig. 2, with  $\Gamma_i = \text{const}$ , the pulse duration appears to be not long enough for the interparticle gap and elasticity modulus to change (Fig. 2d, h, l). Therefore, the particle interaction energy remains almost unchanged (Fig. 2b, f, j) by the end of the pulse and so is the dimer extinction spectrum (Fig. 2a, e, i; curves 2).

In the second case,  $\Gamma_i(T)$  (Fig. 3), again the pulse duration is too short for the dimer configuration and elastic properties of the polymer to change. Yet, due to the increased  $\Gamma_i$  under heating, the extinction spectrum (Fig. 3a, e, i; curve 2) and the optical component of the interaction energy (Fig. 3b, f, j) change dramatically. The energy absorbed by domain particles drastically reduces with growing relaxation constant because of the decreasing Q-factor of plasmon resonance (Fig. 3a, e, i; curve 2). This leads to a drop in electron and ion temperatures (compare Figs. 2 and 3c, g, k).

In both cases, the temperature of electron and ion components of the domain particle reaches its maximum when the laser wavelength coincides with the maximum of the extinction spectrum ( $\lambda = 460 \text{ nm}$ ) (Figs. 2e, 3e). The temperature of the electron component drops once the pulse is over, and after a 20–30-ps delay, the temperature

of the ion component maximizes. It is explained by the finite time (of order  $\sim 10^{-11} \text{ s}$ ) of energy exchange between electrons and the lattice.

In turn, the increase in  $T_i$  results in heating of the polymer adlayer and destruction of molecular bonds therein. This is accompanied by decrease in the elasticity modulus and attraction of particles (Figs. 2h, 3h) under the action of the van der Waals forces mainly after the pulse is over. This behavior of the domain particles leads to a shift of the maximum in the initial extinction spectrum to the long-wavelength range (Figs. 2a, e, 3e, curves 3). Since particles in the case of  $\Gamma_i(T)$  are heated much less than in the case of  $\Gamma_i = \text{const}$ , the elasticity modulus is less reduced, and hence, the particles attract approximately 10 times slower (Fig. 3h).

Changes in the dimer characteristics maintained after the pulse is over (at  $t = 20 \text{ ns}$ ) correspond to photomodification of the dimer called *static* hereinafter. Assume that the *threshold of static photomodification* corresponds to the radiation intensity such that the changes in the optical and structural properties (Figs. 2e, 3e; curve 3 and 2h, 3h) of the dimer are maintained even after the end of the pulse when the laser wavelength coincides with the maximum of extinction spectrum (Figs. 2e, 3e,  $\lambda = 460 \text{ nm}$ , the so called “resonant case”). Note that *static photomodification* is possible to occur when the laser wavelength detunes from the position of the extinction spectrum maximum (see static changes in Fig. 2a, d,  $\lambda = 430 \text{ nm}$ ).

*Dynamic* spectral changes in a dimer over the pulse duration occur as a result of melting of the particle and

disappearance of the plasmon resonance (an abrupt decrease in its Q-factor, to be more exact) (Fig. 3a, i; curves 2) and may precede the *static* ones. Plasmon resonance restores after the pulse is over and the particles cool down (Fig. 3a, i; curves 3), which is manifested in restoration of the structural domain properties (the interparticle gap and elasticity modulus in Figs. 2l, 3d, l)

Thus, there is an evolution of optical and structural properties observed in the dimer, which manifests itself in both *static* (registered long time after the pulse is over) and *dynamic* (registered while the pulse is on) changes in the characteristics of the domain.

### 3.2 Polydisperse domain

Comparative kinetics of basic characteristics of a polydisperse dimer consisting of two different-sized particles, one being four times the size of the other [the case of  $\Gamma_i(T)$ ], is presented in Figs. 4 and 5 for two different radiation intensities. The average particle size corresponds to the size of particles in a monodisperse dimer (simple average size). The distinctive feature of the initial extinction spectrum of a polydisperse dimer is an additional weakly contrasted maximum (Figs. 4, 5a, f, k, curve 1) introducing asymmetry into the plasmon absorption band. Radiation wavelengths also coincide with the short- and long-wavelength wings of the initial extinction spectrum and with its maximum. Calculations were performed for the following laser wavelengths:  $\lambda = 370, 400, 430$  nm, Figs. 4 and 5. Dynamic characteristics shown in the respective columns are the same as described in the previous section but, unlike Figs. 2 and 3, include additionally temperatures of small (*s*) and large (*b*) particles in columns 3 and 4.

Let us start with comparing the changes of characteristics of polydisperse (Fig. 4) and monodisperse dimers (Fig. 3) under the same conditions of irradiation and the radiation intensity corresponding to the threshold of *static photomodification* of a monodisperse dimer ( $I = 7.5 \times 10^8$  W/cm<sup>2</sup>). In the case of  $\Gamma_i(T)$  and  $I = 7.5 \times 10^8$  W/cm<sup>2</sup>, *static* changes (Fig. 4; e, j, o) occur at wavelengths corresponding both to the wings and the maximum of the initial extinction spectrum (Fig. 4a, f, k; curves 3) and are observed during the pulse duration. The extinction spectrum is shifted to the long-wavelength range under *static photomodification* as shown in Fig. 4a, f, k; curves 3. This suggests that the particles keep approaching each other long after the pulses over. Note that the intensity threshold of *static photomodification* is lower for a polydisperse dimer than for a monodisperse dimer and equals  $I = 7.7 \times 10^7$  W/cm<sup>2</sup> (see Fig. 5, f, j). Polydispersity of the dimer causes another effect associated with a different heating rate of different-sized particles. The dipole moment is proportional to the particle volume; therefore, the field

produced by a large particle in the location of a smaller one is higher than the field generated by a small particle at the location of a larger one. This leads to a faster heating of the small particle (for more details see “Appendix”), resulting in a decreased threshold of photomodification.

On the contrary, *dynamic* changes in a polydisperse dimer during the laser pulse are accompanied by a shift of the extinction spectrum (unlike a monodisperse dimer where spectral changes cause the Q-factor of plasmon resonance to decrease) to the short-wavelength range (Figs. 4k, 5a, f, k, curve 2). This is due to melting of the small particle while the crystal lattice of the larger particle remains unaffected. The resultant single resonance (Figs. 4k, 5a, f, k, curve 2) corresponds to the initial resonance of a large isolated particle. Its emergence is due to an abrupt decrease in the Q-factor of the plasmon resonance of the small particle (while that of the larger one remains unchanged), which is accompanied by weakening of the electrodynamic interaction of particles in a pair. This strongly modifies the extinction spectra of particles under normal conditions (curve 1 in Figs. 4 and 5a, f, k).

Figures 3 and 4 allow us to compare photomodification of monodisperse and polydisperse dimers accompanied by an abrupt decrease in the Q-factor of plasmon resonance under similar conditions (Figs. 3, 4a, f, curve 2).

Maximum temperatures of electron and ion components (Figs. 4, 5h, i) in a polydisperse domain (when the radiation intensity corresponds to the threshold of static photomodification of monodisperse and polydisperse domains, respectively) take place when the laser wavelength coincides with the maximum of the initial extinction spectrum (Figs. 4, 5f). Under these conditions, a heated metal core induces heating and melting of the polymer adlayer and causes the particles to approach each other (Figs. 4, 5j) under the action of van der Waals forces after the end of the pulse. This is accompanied by the shift of the extinction spectrum to the long-wavelength range (Figs. 3e, 4f, 5f; curve 3). Spectral *dynamic* changes during the pulse occur as in the case of a monodisperse dimer because of melting of particles and disappearance of plasmon resonance (see curve 2 of Figs. 3e, and 4f).

Thus, both *dynamic* and *static* changes of the extinction spectrum are observed in monodisperse as well as polydisperse domain.

Comparative spectra of monodisperse and polydisperse dimers at intensities below the static photomodification threshold and yet causing dynamic changes in the properties of the dimers are shown in Fig. 6 [the case of  $\Gamma_i(T)$ ]. Decreasing the radiation intensity down to  $2.7 \times 10^7$  W/cm<sup>2</sup> in the case of a monodisperse dimer does not lead to any significant change of its properties due to low temperature of the metallic cores of particles. Slight dynamic changes in the spectrum (Fig. 6f, curve 2) at temperatures

above the melting threshold of particles (Fig. 6g) are only observed under resonant excitation. Once the pulse is over, the dimer spectrum recovers its initial shape.

In a polydisperse dimer, radiation of the same intensity causes only dynamic photomodification which is, however, more pronounced. This is due to melting of small particles (Fig. 6d, i, n) and weakening of the resonant interaction of particles in the dimer resulting in a dynamic shift of the extinction spectrum to the short-wavelength range (Fig. 6c, h, m, curve 2). This spectrum corresponds to the spectrum of a large single particle at the end of the laser pulse. The initial spectrum recovery is due to cooling of the small particle below the melting temperature and restoration of the quality factor of plasmon resonance of the small particle and resonant electromagnetic interactions between large and small particles (Fig. 6c, h, m, curve 3). There is no shift of dimer particles and therefore the dimer extinction spectrum is restored to the initial one.

When estimating frequency shift during dynamic photomodification, it is also necessary to take into account the correction for the shift of particle plasmon frequency ( $\omega_{pl}$ ) related to a change in the permittivity  $\varepsilon_m$  of environment when the vapor cavity is formed around a particle (see for example [45, 46], theoretical model of this phenomenon see in [47]), because  $\omega_{pl} \sim (\varepsilon_a + 2\varepsilon_m)^{-1/2}$ , where  $\varepsilon_a$  is contribution of interband transitions (for Ag  $\varepsilon_a \approx 5$  [1]). However, maximal frequency shift for steam and water  $\omega_{pl}(\varepsilon_m \geq 1)/\omega_{pl}(\varepsilon_m = 1.78) \leq 1.11$  is insignificant (experimentally registered shift in these conditions is equal to 18 nm [46]) for dynamic photomodification, and it has no effect for static photomodification when steam bubble disappears after the pulse is over.

Note that unlike air medium [47–49], silver nanoparticles in hydrosols are well preserved and are not subjected to rapid oxidation, that is, evidenced by the manifestation of the plasmon absorption of hydrosols for many months.

It should be noted that our model can be easily modified by taking into account these and other effects, which allows one to receive more adequate and accurate results.

## 4 Summary

Using the elaborated optodynamical model, we have studied the behavior of interaction between a picosecond laser pulse and the simplest domains of multiparticle Ag aggregates—dimers.

In our model, we are the first to take into account temperature dependence of the electron relaxation constant of the particle material and the effect of this factor on interaction of laser radiation with aggregates of nanoparticles. It was found that this leads to dramatic changes in the interpretation of optodynamics and optical

characteristics of bound nanoparticles and totally alters our idea of the process of interaction of radiation with bound metal particles.

Taking into consideration polydispersity of particles in the dimer revealed an important feature: a small particle is heated faster than a larger one, which leads to decrease in Q-factor of plasmon resonance of the small particle and suppression of resonant interaction with the large particle. This results in the appearance of a resonant band of a single large particle in the extinction spectrum.

Optical forces were shown to make a significant contribution comparable with the van der Waals forces only at high light intensity achieved in picosecond pulses. But during such a short time, optical forces cannot shift particles in domain. In long nanosecond pulses, the effect of optical forces is negligible due to low light intensity.

The static photochromic effect in disperse systems containing colloidal aggregates of plasmonic nanoparticles was shown to cause irreversible light-induced movement of nanoparticles in resonant domains in multiparticle aggregates and change the resonant properties of domains in pulsed laser fields. The dynamic changes are due to melting of the metallic core of particles and a subsequent decrease in the Q-factor of plasmon resonance during the laser pulse; and this may be associated with the increase in the electron relaxation constant of metal. The possibility of manifestation of reversible effects occurring after the laser pulse has been shown.

The model developed is universal and can be applied to study any type of disperse systems interacting with pulsed laser radiation.

**Acknowledgments** Authors are thankful to Prof. V. A. Markel (University of Pennsylvania) for supplying program codes for realization of the coupled dipole method for polydisperse metal nanoparticle aggregates. This research was supported by the Russian Academy of Sciences under the Grants 24.29, 24.31, III.9.5, 43, SB RAS-SFU (101); Ministry of Education and Science of Russian Federation under Contract 14.B37.21.0457.

## Appendix: The heating rate of particles in a polydisperse dimer

Consider a polydisperse dimer ( $R_2 < R_1$ ,  $R_1$ ,  $R_2$  are the radii of dimer particles) in the external field  $\mathbf{E}_0$ . The heating rate is determined by the absorbed power density

$$dT/dt \sim W/R^3, \quad W \sim |\mathbf{d}|^2 \text{Im} \left( \frac{1}{\alpha^*} \right) \quad (37)$$

where  $W$  is the power of radiation absorbed by the particle. Compare the heating rates of the particles. The interaction of particles will be considered in dipole approximation. We assume that

$$(\omega_{pl})_{1,2} \gg \Gamma_2 > \Gamma_1 \quad u \quad (\omega_{pl})_1 \approx (\omega_{pl})_2 = (\omega_{pl}) \quad (38)$$

that is, the surface plasmon resonances of both particles differ very little. Hence, for the dipole moments of the particles, we can write down:

$$|\mathbf{d}_1| = \varepsilon_m |\alpha_1| \cdot |\mathbf{E}_0 + \mathbf{E}_2|, \quad |\mathbf{d}_2| = \varepsilon_m |\alpha_2| \cdot |\mathbf{E}_0 + \mathbf{E}_1|,$$

$$\mathbf{E}_1 = \frac{2\mathbf{d}_1}{\varepsilon_m r_{12}^3}, \quad \mathbf{E}_2 = \frac{2\mathbf{d}_2}{\varepsilon_m r_{12}^3}, \quad (39)$$

where  $\mathbf{E}_1$  and  $\mathbf{E}_2$  are the fields produced by the first and the second particle at the location of the neighboring one,  $r_{12} = R_1 + R_2 + h_{ij}$ ,  $h_{ij}$  is the interparticle gap. Substituting (39) into (37) yields

$$\frac{W_1}{R_1^3} \sim \varepsilon_m^2 \frac{|\alpha_1|^2}{R_1^3} |\mathbf{E}_0|^2 \left| 1 + \frac{2\alpha_2}{r_{12}^3} \right|^2 \cdot \text{Im} \left( \frac{1}{\alpha_1^*} \right),$$

$$\frac{W_2}{R_2^3} \sim \varepsilon_m^2 \frac{|\alpha_2|^2}{R_2^3} |\mathbf{E}_0|^2 \left| 1 + \frac{2\alpha_1}{r_{12}^3} \right|^2 \cdot \text{Im} \left( \frac{1}{\alpha_2^*} \right). \quad (40)$$

Polarizability of the particles  $\alpha_{1,2} = \chi'_{1,2} - i\chi''_{1,2}$  at  $\omega \approx \omega_{pl}$  can be represented as [4]:

$$\alpha_{1,2} = -i\chi''_{1,2}, \quad \chi''_{1,2} = r_{1,2}^3 \frac{\omega_{pl}}{\Gamma_{1,2}}. \quad (41)$$

The specific absorbed power is found by substituting (41) into (40):

$$\frac{W_1}{R_1^3} \sim \varepsilon_m^2 \left( \frac{\omega_{pl}}{\Gamma_1} \right) |\mathbf{E}_0|^2 \left| 1 - i \frac{2\omega_{pl}}{\Gamma_2} \cdot \frac{r_2^3}{r_{ij}^3} \right|^2,$$

$$\frac{W_2}{R_2^3} \sim \varepsilon_m^2 \left( \frac{\omega_{pl}}{\Gamma_2} \right) |\mathbf{E}_0|^2 \left| 1 - i \frac{2\omega_{pl}}{\Gamma_1} \cdot \frac{r_1^3}{r_{ij}^3} \right|^2. \quad (42)$$

Hence, the heating rates will relate as:

$$\frac{W_2/R_2^3}{W_1/R_1^3} \approx \frac{\Gamma_2}{\Gamma_1} \cdot \frac{\Gamma_1^2 + 4\omega_{pl}^2(R_1/r_{12})^6}{\Gamma_2^2 + 4\omega_{pl}^2(R_2/r_{12})^6}. \quad (43)$$

Using (43) for our case, we obtain:  $R_1 = 8$  nm,  $R_2 = 2$  nm,  $r_{12} = 11$  nm,  $\omega_{pl} = 4.7 \times 10^{15} \text{ s}^{-1}$ ,  $\Gamma_{1,2} = \Gamma_\infty + \frac{\nu_E}{r_{1,2}}$ ,  $\Gamma_\infty = 1.5 \times 10^{14} \text{ s}^{-1}$ ,  $\Gamma_1 = 3.25 \times 10^{14} \text{ s}^{-1}$ ,  $\Gamma_2 = 8.5 \times 10^{14} \text{ s}^{-1}$ . As the result  $(W_2/R_2^3)/(W_1/R_1^3) \approx 47$ . That is, the initial heating rate of the small particle is much higher than that of the large particle.

### References

1. U. Kreibig, M. Vollmer, *Optical Properties of Metal Clusters* (Springer, Berlin, 1995)
2. V.M. Shalaev, Phys. Rep. **272**, 61 (1996)
3. V.M. Shalaev, *Nonlinear Optics of Random Media: Fractal Composites and Metal-Dielectric Films* (Springer, Berlin, 2000)

4. S.V. Karpov, V.V. Slabko, *Optical and Photophysical Properties of Fractal-Structured Metal Sols* (Russian Academy of Sciences, Siberian Branch, Novosibirsk, 2003)
5. M.I. Stockman, L.N. Pandey, T.F. George, *Enhanced Nonlinear Optical Responses of Disordered Clusters and Composites in Nonlinear Optical Materials* (Springer, New York, 1998)
6. A.P. Gavriluk, S.V. Karpov, Appl. Phys. B **97**, 163 (2009)
7. S.V. Karpov, A.K. Popov, S.G. Rautian, V.P. Safonov, V.V. Slabko, V.M. Shalaev, M.I. Shtokman, JETP Lett. **48**, 571 (1988)
8. E.Y. Danilova, S.G. Rautian, V.P. Drachev, S.V. Perminov, Bull. Russ. Acad. Sci. (Phys.) **60**, 18 (1996)
9. E.Y. Danilova, S.G. Rautian, V.P. Safonov, Bull. Russ. Acad. Sci. (Phys.) **60**, 56 (1996)
10. V.P. Safonov, V.M. Shalaev, V.M. Markel, Y.E. Danilova, N.N. Lepeskin, W. Kim, S.G. Rautian, R.L. Armstrong, Phys. Rev. Lett. **80**, 1102 (1998)
11. S.V. Karpov, V.V. Slabko, A.K. Popov, Tech. Phys. **48**, 749 (2003)
12. S.V. Karpov, M.K. Kodirov, A.I. Rysanyanski, V.V. Slabko, Quantum Electron. **31**, 904 (2001)
13. S.V. Karpov, V.S. Gerasimov, I.L. Isaev, V.A. Markel, Phys. Rev. B **72**, 205425 (2005)
14. S.V. Karpov, V.S. Gerasimov, I.L. Isaev, O.P. Podavalova, V.V. Slabko, Colloid J. **69**, 178 (2007)
15. A.P. Gavriluk, S.V. Karpov, Appl. Phys. B **102**, 65 (2011)
16. V.P. Drachev, S.V. Perminov, S.G. Rautian, V.P. Safonov, J. Exp. Theor. Phys. **94**, 901 (2002)
17. S.V. Perminov, V.P. Drachev, S.G. Rautian, Opt. Express **15**, 8639 (2007)
18. S.V. Perminov, V.P. Drachev, S.G. Rautian, Opt. Lett. **33**, 2998 (2008)
19. S.V. Perminov, V.P. Drachev, Opt. Spectrosc. **107**, 987 (2009)
20. S.V. Karpov, V.V. Slabko, G.A. Chiganova, Colloid J. **64**, 474 (2002)
21. J. Možina, J. Diaci, Appl. Phys. B **105**, 557 (2011)
22. J. Možina, R. Hrovatin, Prog. Nat. Sci. **6**, S709 (1996)
23. R.A. Ganeev, A.I. Rysanyanski, S.R. Kamalov, M.K. Kodirov, T.J. Usmanov, Phys. D Appl. Phys. **34**, 1602 (2001)
24. V.A. Podolskiy, A.K. Sarychev, E.E. Narimanov, V.M. Shalaev, J. Opt. A **7**, 32 (2005)
25. V.A. Markel, A.K. Sarychev, Phys. Rev. B **75**, 085426 (2007)
26. A.A. Govyadinov, V.A. Markel, Phys. Rev. B **78**, 035403 (2008)
27. W.H. Weber, G.W. Ford, Phys. Rev. B **70**, 125429 (2004)
28. S.V. Karpov, I.L. Isaev, A.P. Gavriluk, A.S. Grachev, V.S. Gerasimov, Colloid J. **71**, 314 (2009)
29. L.D. Landau, E.M. Lifshits, *The Theory of Elasticity. Course of Theoretical Physics* (Nauka, Moscow, 1987)
30. Y.S. Barash, *The van der Waals Forces* (Nauka, Moscow, 1988)
31. F. Claro, R. Rojas, Appl. Phys. Lett. **65**, 2643 (1994)
32. V.A. Markel, V.M. Shalaev, E.B. Stechel, W. Kim, R.L. Armstrong, Phys. Rev. B **53**, 2425 (1996)
33. V.A. Markel, V.N. Pustovit, S.V. Karpov, A.V. Obuschenko, V.S. Gerasimov, I.L. Isaev, Phys. Rev. B **70**, 054202 (2004)
34. A.E. Ershov, I.L. Isaev, P.N. Semina, V.A. Markel, S.V. Karpov, Phys. Rev. B **85**, 045421-1 (2012)
35. P.B. Johnson, R.W. Christy, Phys. Rev. B **6**, 4370 (1972)
36. C. Kittel, *Introduction to Solid State Physics* (Wiley, New York, 1971)
37. M. Otter, Z. Phys. **161**, 539 (1961)
38. J.C. Miller, Philos. Mag. **20**, 1115 (1969)
39. O.B. Wright, Phys. Rev. B **49**, 9985 (1994)
40. T. Castro, R. Reifengerber, E. Choi, R.P. Andres, Phys. Rev. B **42**, 8548 (1990)
41. C.-K. Sun, F. Vallée, L.H. Acioli, E.P. Ippen, J.G. Fujimoto, Phys. Rev. B **50**, 15337 (1994)

42. N. Del Fatti, C. Voisin, M. Achermann, S. Tzortzakis, D. Christofilos, F. Vallée, *Phys. Rev. B* **61**, 16956 (2000)
43. R. Groeneveld, R. Sprik, A. Lagendijk, *Phys. Rev. B* **51**, 11433 (1995)
44. Y.A. Frenkel, *The Kinetic Theory of Liquids* (Nauka, Moscow, 1975)
45. A.A. Chastov, O.L. Lebedev, *J. Exp. Theor. Phys.* **58**, 848 (1970)
46. Z. Fang, Y.-R. Zhen, O. Neumann, A. Polman, F. Javier García de Abajo, P. Nordlander, N.J. Halas, *Nano Lett.* **13**, 1736 (2013)
47. V.K. Pustovalov, I.A. Khorunzhii, D.S. Bobuchenko, *Bull. Acad. Sci. USSR Phys.* **52**, 1847 (1988)
48. M.D. McMahon, R. Lopez, H.M. Meyer III, L.C. Feldman, R.F. Haglund Jr., *Appl. Phys. B* **80**(7), 915 (2005)
49. W. Cao, H.E. Elsayed-Ali, *Mater. Lett.* **63**, 26–2263 (2009)